https://doi.org/10.5194/egusphere-2024-2899
Preprint. Discussion started: 25 September 2024

Emplacement age of the Sevier Gravity Slide, Utah, USA

Tiffany Rivera[1], McKenna Holliday[2], Brian Jicha[3], David H. Malone[4], Michael J. Braunagel[5], V. Alex Bonilla Franco[6], Robert F. Biek[7], W. Ashley Griffith[8], David B. Hacker[9]

[1] Department of Geological Sciences, University of Missouri, Columbia, 65201, USA
[2]Department of Geological Sciences, University of Florida, Gainesville, 32603, USA
[3]Department of Geoscience, University of Wisconsin-Madison, Madison, 53706, USA
[4]Department of Geography, Geology and the Environment, Illinois State University, Normal, 61790, USA
[5]Department of Earth & Environmental Sciences, University of Minnesota Duluth, 55812
[6]Department of Geological Sciences, Jackson School of Geosciences, University of Texas, Austin, 78712, USA
[7]Utah Geological Survey, Salt Lake City, 84116, USA, retired
[8]School of Earth Sciences, Ohio State University, Columbus, 43210, USA
[9]Department of Geology, Kent State University, Kent, 44242, USA

Correspondence to: Tiffany A. Rivera (trivera@missouri.edu)

https://doi.org/10.5194/egusphere-2024-2899
Preprint. Discussion started: 25 September 2024

Abstract. The Marysvale volcanic field in southwestern Utah hosts three large volume gravity slides: the Sevier (SGS), the Markagunt (MGS), and the Black Mountains (BGS). The gravity slides are composed of lahar deposits, lava flows, and ash-flow tuffs erupted from former stratovolcanoes and other vents during the Oligocene and Miocene. The ash-flow tuffs are prime targets for dating to constrain the age of the gravity slides because some ash-flow tuffs are deformed within the slides, whereas others are undeformed and cap the slides. Furthermore, the gravity slides produced pseudotachylyte during slide motion, a direct indicator for the timing of each slide. This work provides new $^{40}Ar/^{39}Ar$ dates for several ash-flow tuffs and pseudotachylyte for the SGS, along with U/Pb zircon dates for one deformed tuff and overlying alluvium at the slide plane. Results show that the slide was emplaced at 25.25 ± 0.05 Ma and was immediately followed by the eruption of the Antimony Tuff at 25.19 ± 0.02 Ma. The model presented here suggests that the intrusion of magma related to the Antimony Tuff acted as a triggering mechanism for the slide, and that slide movement itself led to decompression melting and eruption of the Antimony Tuff. This sequence of events occurred on a geologically rapid timescale and may have been virtually instantaneous.

Short summary. The timing of an ancient gravity slide that originated in the Marysvale volcanic field (Utah) is constrained using $^{40}Ar/^{39}Ar$ dating of pseudotachylyte, a friction-induced glass that is generated during slide movement, and the volcanic tuffs that were displaced by the slide and those that overly the slide mass. Our results suggest that the Sevier gravity slide occurred at 25.25 Ma. The removal of such a large volume of material likely allowed for the eruption of the Antimony Tuff at 25.19 Ma.

1 Introduction

Gravity slides are large volume mass movements that typically slide over shallowly dipping (≤ 3˚) paleosurfaces. The Heart Mountain slide (Wyoming) and the recently described Markagunt Gravity Slide (Utah) were coeval with volcanism and displaced km-thick sheets of volcanic rocks (Biek et al., 2022; Malone, 1995; Malone et al., 2017). A characteristic feature of gravity slides is that they maintain the original stratigraphy within the allochthonous sheets. The presence of volcanic materials offers opportunities to constrain the emplacement age using several geochronological techniques. Furthermore, these megaslides are emplaced so rapidly that they can generate pseudotachylyte, a friction induced melt hypothesized to have formed from the rocks involved in sliding. Geochronology of the pseudotachylyte can directly constrain the age of the slide.

The Oligocene-Miocene Marysvale gravity slide complex (MGSC) in southwestern Utah is unique in that it contains multiple, gigantic individual gravity slides, including the Sevier gravity slide (SGS), the 23 Ma Markagunt gravity slide (MGS; (Holliday et al., 2022)), and the Black Mountain gravity slide (BGS) (Biek et al., 2019, 2022). Despite the coeval nature of the MGSC and the Marysvale Volcanic Field (MVF), the causality of gravity slide emplacement is still unclear. Slide initiation may be due to magmatic doming within the gravity slide's breakaway region, laccolith emplacement, or the accumulation of volcanic material on weak strata may overload the crust and stimulate widespread slope failure (Hacker et al., 2018). Recent work has improved the understanding about source

https://doi.org/10.5194/egusphere-2024-2899
Preprint. Discussion started: 25 September 2024

material and kinematics of these landslides (Braunagel et al., 2023; Hacker et al., 2023; Holliday et al., 2022; Zamanialavijeh et al., 2021). Notably, Holliday et al. (2022) obtained $^{40}Ar^*/^{39}Ar$ dates on the ash-flow tuffs and pseudotachylyte from the MGS, then employed a novel Bayesian statistical optimization age model to constrain an emplacement age. This work builds upon the previous geochronology study of the MGS to determine the emplacement age of the SGS through $^{40}Ar^*/^{39}Ar$ dating of pseudotachylyte formed during slide movement and of the bounding ash-flow tuffs. Our results unambiguously tie pseudotachylyte formation to slide emplacement, affirming the catastrophic nature of the slides, while simultaneously constraining the timing of slope failure relative to volcanic eruptions, which resolves outstanding questions surrounding causality of gravity slides.

2 Geologic background

Early investigations in the MVF have provided the foundation for the discovery of the MGSC and unraveling the associated stratigraphy as described in Biek et al. (2019). Geochemical investigations of the volcanic units led to the identification of the calc-alkaline nature of the older rocks and bimodal basalt and high-silica rhyolite younger rocks (Rowley et al., 1975; Steven et al., 1977; Wender and Nash, 1979), and extensive mapping initiatives were undertaken to unravel the geology, mineral resources, and economic potential of the region (e.g., Steven et al., 1977; Cunningham and Steven, 1979; Steven et al., 1984; Palmer and Walton, 1990; Rowley et al., 1994; Rowley et al., 1998; Granger and Bauer, 1950; Taylor et al., 1951; Kerr et al., 1957; among many others). This foundational body of work contributes to understanding the spatial distribution of the volcanic centers and the stratigraphic relationships between major eruptive units. The MVF straddles the boundary between the Colorado Plateau and the Basin and Range province and covers >10,000 km^2, with an estimated total volume of 12,000 km^3 (Rowley et al., 1998), and hosts three calderas: Three Creeks (~27 Ma), Monroe Peak (23–22 Ma), and Mount Belknap (22–18 Ma). However, most of the eruptive products in the MVF have an unknown source, presumably because many vent areas are now buried or overprinted by younger calderas. The breakaway regions for each gravity slide are inferred to be entirely within the MVF, and suggest a genetic connection to local volcanic activity. The breakaway zones of the SGS and MGS are overprinted by younger calderas (Rowley et al., in press; Biek et al., 2019, 2022), and the breakaway of the BGS has presumably been eroded over the Mineral Mountains batholith.

Initiation of MVF volcanism is associated with Farallon slab rollback and southward migration of volcanism across western North America. Peak volcanic (23–32 Ma) activity consisted of intermediate calc-alkaline eruptions (Rowley et al., 1998; 2002; in press) which account for ~90% of the MVF volcanic material contained in the Bullion Canyon Volcanics and the Mount Dutton Formation (Rowley et al., 1994). The transition to bimodal basalt and high-silica rhyolite volcanism occurred ca. 22 Ma and is linked to the transition from a subduction-style regime to Basin and Range extension (Rowley et al., 1997). Basaltic eruptions have continued into the late Pleistocene (Biek et al., 2015; Marchetti et al., 2020).

Recognition of the MGSC began with the early characterization of the Markagunt Megabreccia on the Markagunt Plateau (Anderson, 1993). Described as isolated allochthonous masses (megabreccia), the Markagunt Megabreccia consists of monolithic blocks and heterolithologic complexes as large as 2.5 km^2 and 50–200 m thick

https://doi.org/10.5194/egusphere-2024-2899
Preprint. Discussion started: 25 September 2024

(Sable and Maldonado, 1997). While these large masses were identified as gravity slides, they were interpreted to be emplaced in several separate events from multiple sources (Anderson, 1993; Sable and Maldonado, 1997). However, Hacker et al. (2014) and Biek et al. (2014; 2015) reinterpreted the Markagunt Megabreccia as part of a catastrophically emplaced single slide mass based on new field evidence and mapping, and termed this the Markagunt gravity slide (MGS). The Sevier gravity slide (SGS) was proposed in 2017 (Biek et al., 2017), and formally recognized in Biek et al. (2019). Along the western flank of the SGS, Braunagel et al. (2023) characterized notable structural features that indicate intense deformation, clastic dikes of basal material into overlying rocks, pseudotachylyte, and cataclastic basal zones. Loffer (2024) identified several pseudotachylyte sites within the SGS, and proposed an SGS maximum depositional age of 25.5 Ma using detrital zircon extracted from the basal layer of the slide in two locations.

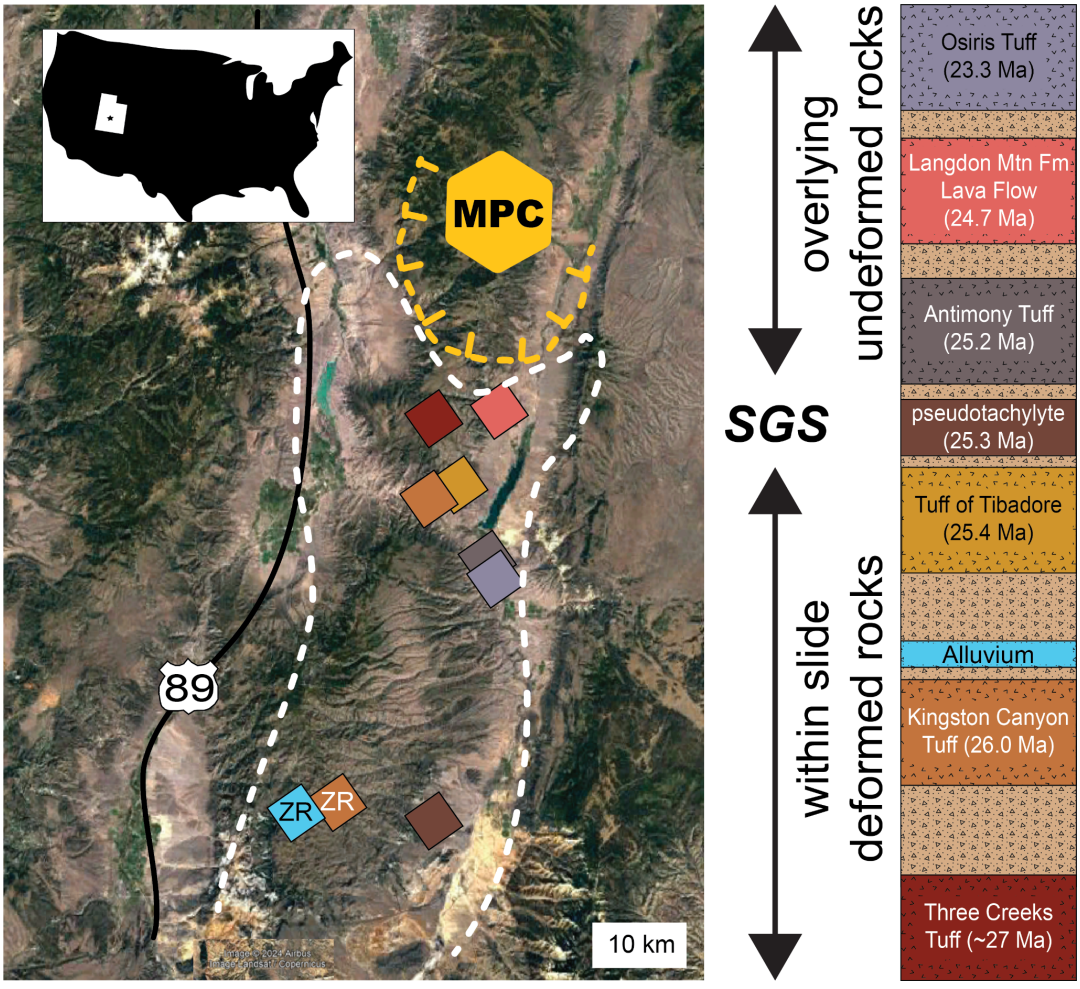

Figure 1: Sevier gravity slide location (white boundary) shown with Monroe Peak Caldera (MPC) and sampling locations. To the right, a simplified stratigraphic section (not to scale) of the Mount Dutton Formation (light brown) with interspersed

https://doi.org/10.5194/egusphere-2024-2899
Preprint. Discussion started: 25 September 2024

ash-flow tuffs and other rocks investigated in this study. The allochthonous block of the SGS includes the within slide deformed ash-flow tuffs and pseudotachylyte, whereas the overlying undeformed ash-flow tuffs post-date slide emplacement. Locations labeled with "ZR" indicate samples collected for zircon U/Pb dating. © Google Earth, using 2024 imagery of Airbus, Landsat, Conpernicus.

3 Materials and methods

The units investigated here are grouped by their stratigraphic position relative to the SGS. Ash-flow tuffs 'within' the slide material are deformed and were displaced by slide motion as an allochthonous block. Ash-flow tuffs 'above' the slide are all undeformed by and postdate the SGS (Fig. 1). The Kingston Canyon Tuff (samples 21MGSC-02 and KCT; Fig. 2) is a densely welded, red-purple, lithic tuff. Plagioclase is the major mineral phase, with minor hornblende and biotite. Lithic components consist of mafic igneous rocks. A sample of the alluvial facies of the Mt. Dutton Formation overlying the KCT sample was collected to examine the detrital zircon record (MVC6-21-10-16-2; Braunagel et al., in review). The tuff of Tibadore (21MGSC-01, Fig. 2) is a crystal poor, densely welded lithic ash-flow tuff. Fresh surfaces are purple with black fiamme 1–3 cm long. The Antimony Tuff (PH030218-1, Fig. 2) is a densely welded, relatively crystal-poor ash-flow tuff, with a red groundmass containing large plagioclase, minor pyroxene, and lithics. The Langdon Mountain Formation contains a lower lahar facies and an upper lava flow facies; only the lava flow facies, dated here, clearly postdates the SGS (Rowley et al., 2002). The lava flow facies is described as a dacitic lava flow containing large phenocrysts of plagioclase, hornblende, and minor pyroxene (Rowley et al., in press) and considered the last of the minor eruptive sequences prior to the eruption of the caldera-forming Osiris Tuff (Rowley et al., 1994); eruptive vents of the Langdon Mountain rocks were likely destroyed by emplacement of the Monroe Peak caldera. The Osiris Tuff (PH030218-2) contains dominantly large feldspar phenocrysts, conspicuous biotite, and minor pyroxene within a gray groundmass. The Osiris Tuff is not deformed by the SGS, but was deformed by the later 23 Ma MGS emplacement near the breakaway zone at Puffer Lake (Biek et al., 2019; Holliday et al., 2022). Pseudotachylyte (24MSGC-37, Fig. 2) is found on shear planes and in injection veins as much as 200 m above the basal slip surface.

https://doi.org/10.5194/egusphere-2024-2899
Preprint. Discussion started: 25 September 2024

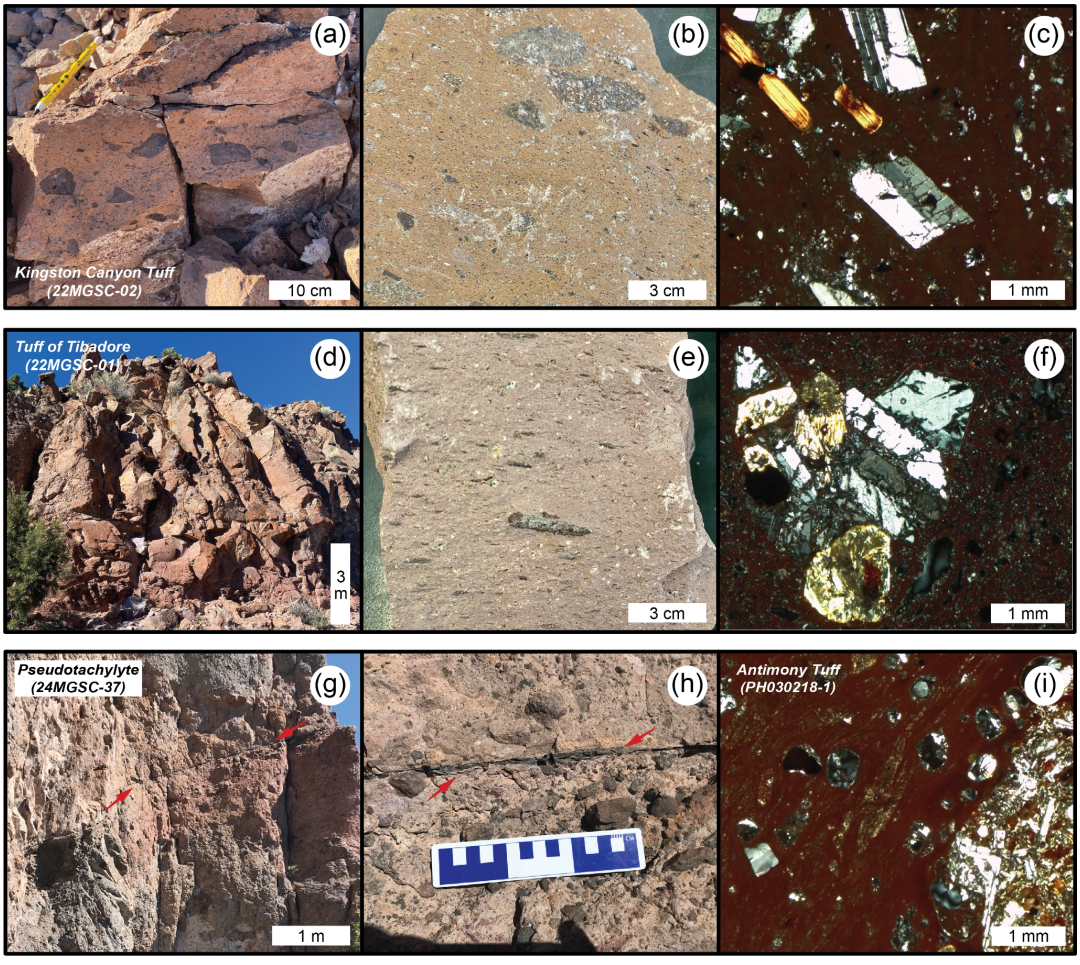

Figure 2: (a) Outcrop of Kingston Canyon Tuff; (b) Hand sample of Kingston Canyon Tuff showing abundant lithic fragments; (c) thin section of Kingston Canyon Tuff showing plagioclase and biotite phenocrysts; (d) outcrop of tuff of Tibadore; (e) tuff of Tibadore hand sample with prominent fiamme; (f) thin section of the tuff of Tibadore showing rare crystal clot; (g) outcrop of pseudotachylyte vein; (h) outcrop of pseudotachylyte vein; (i) thin section of Antimony Tuff showing mafic xenolith (right side of image) and fiamme. Thin section photographs were taken in crossed polarized light.

3.1 $^{40}Ar/^{39}Ar$ analysis

Samples of each ash-flow tuff, lava flow, and pseudotachylyte described above were processed by standard crushing, magnetic, and density techniques to prepare for $^{40}Ar/^{39}Ar$ analysis. Sanidine was extracted from the Osiris and Antimony Tuffs, and plagioclase was analyzed from the tuff of Tibadore, Kingston Canyon Tuff, and Langdon Mountain lava flow. Pseudotachylyte glass was handpicked prior to analysis. Selected materials were co-irradiated with the 28.201 Ma Fish Canyon Tuff sanidine neutron fluence monitor (Kuiper et al., 2008) at the Cd-lined facility

https://doi.org/10.5194/egusphere-2024-2899
Preprint. Discussion started: 25 September 2024

at the Oregon State University TRIGA reactor. Single crystal total fusion analyses were conducted for the ash-flow tuffs whereas incremental heating experiments were conducted for the lava flow and pseudotachylyte. All analyses were performed at the WiscAr Geochronology Lab, University of Wisconsin-Madison using either the Noblesse 5 Collector (Jicha et al., 2016) or the Isotopx NGX-600 mass spectrometers (Mixon et al., 2022).

3.2 Zircon U/Pb analysis

Zircon crystals were extracted by traditional methods of crushing and grinding, followed by separation by panning, heavy liquids, and a Frantz magnetic separator. A large split of grains is incorporated into a 1" epoxy mount together with fragments or loose grains of Sri Lanka, FC-1, and R33 zircon crystals that are used as primary standards. The mounts are sanded down to a depth of ~20 microns, polished, imaged, and cleaned prior to isotopic analysis. Grains of interest are imaged to provide a guide for locating analysis pits in optimal locations, and to aid in interpreting results. BSE and color CL Images are generated with a Hitachi 3400N SEM and a Gatan CL2 detector system. U/Pb geochronologic analyses were conducted by laser ablation inductively coupled plasma mass spectrometry (LA-ICPMS) at the Arizona LaserChron Center (www.laserchron.org). Methods for U/Pb geochronology have been described by Gehrels et al. (2006, 2008), Gehrels and Pecha (2014), Pullen et al. (2018), and Sundell et al. (2021).

4 Results

4.1 $^{40}Ar/^{39}Ar$ geochronology

Thirty-three plagioclase crystals from the Kingston Canyon Tuff (21MGSC-02) generated a range of radiogenic yields. As such, only the seven grains with >70% $^{40}Ar^{*}$ were used to calculate the weighted mean and associated statistics. The seven grains yield ages from 25.88 ± 0.06 Ma to 26.08 ± 0.08 Ma and produce a weighted mean of 25.97 ± 0.06 Ma (n = 7/33; MSWD = 1.27). All uncertainties reported in this work include errors associated with the irradiation parameter, J. Nine single crystal plagioclase fusion analyses from the tuff of Tibadore (21MGSC-01) yielded dates from 25.33 ± 0.01 Ma to 25.91± 0.08 Ma. However, in order to filter the data in a consistent manner, analyses with <70% $^{40}Ar^{*}$ were omitted from calculations. Thus a weighted mean for five of the analyses is 25.43 ± 0.05 Ma (MSWD = 0.74). Incremental heating of pseudotachylyte glass (24MGSC-37) produced a plateau age of 25.25 ± 0.05 Ma including >85% of the cumulative $^{39}Ar_K$. The $^{40}Ar/^{36}Ar$ isochron intercept of 292.4 ± 8.8 is within uncertainty of the atmospheric value (Lee et al., 2006). Two locations were sampled for Antimony Tuff and sanidine from both were analyzed by total fusion. Thirteen grains from sample PH030218-1 produced dates ranging from 25.02 ± 0.07 Ma to 25.26 ± 0.07 Ma. A weighted mean of these yields an age of 25.14 ± 0.06 Ma (MSWD = 1.33). Twenty-seven sanidine grains from sample (MP071020-2) produced dates ranging from 25.14 ± 0.03 Ma to 25.23 ± 0.03 Ma, and a weighted mean of these produce an age of 25.19 ± 0.02 Ma (MSWD = 1.45). Combining the two datasets and applying normalized Median Absolute Deviation (nMAD) filter of 1.5 (e.g., Kuiper et al., 2008), 35 of the 40 total grains produce a weighted mean age of 25.19 ± 0.02 Ma (MSWD = 1.17). Bulk

https://doi.org/10.5194/egusphere-2024-2899
Preprint. Discussion started: 25 September 2024

plagioclase from the Langdon Mountain lava flow was incrementally heated and produced a plateau age of 24.68 ± 0.32 Ma with 100% of the cumulative $^{39}Ar_K$. The $^{40}Ar/^{36}Ar$ isochron intercept of 299.3 ± 10.3 is within uncertainty of the atmospheric value (Lee et al., 2006). Holliday et al. (2022) report total fusion dates of thirteen sanidine grains from the Osiris Tuff, which produced dates ranging from 23.16 ± 0.08 Ma to 23.37 ± 0.04 Ma and a weighted mean age of 23.27 ± 0.05 Ma (MSWD = 1.60).

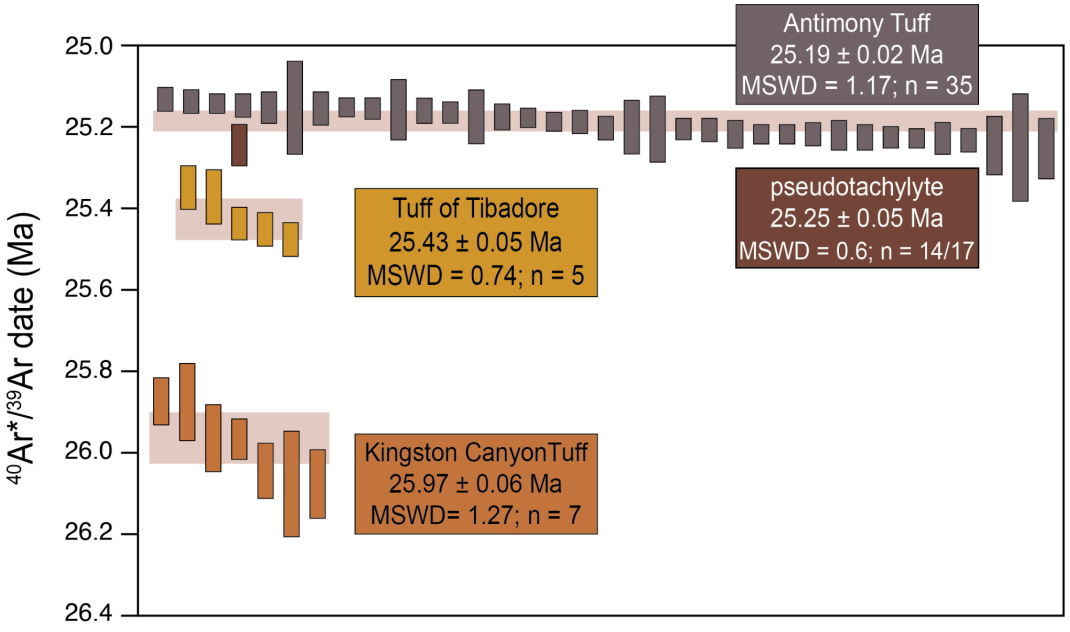

Figure 3: Results of single crystal fusion $^{40}Ar/^{39}Ar$ analyses for the volcanic units overlying and within the Sevier gravity slide, and incremental heating result of the slide-generated pseudotachylyte. Height of each bar represents the $^{40}Ar/^{39}Ar$ date and 2σ uncertainty of a single experiment. The height of the shaded region behind Kingston Canyon Tuff, tuff of Tibadore, and Antimony Tuff represents the weighted mean with 2σ uncertainty of the shown analyses. n = number of single crystal analyses used to calculate the weighted mean, except for the pseudotachylyte, in which n refers to the number of incremental heating steps used to calculate a plateau age.

4.2 Zircon U/Pb geochronology

Zircon $^{206}Pb^*/^{238}U$ dates from the Kingston Canyon Tuff (sample KCT) range from 25.11 ± 0.37 Ma to 1871 ± 12 Ma (n = 122; supplementary materials). Precambrian grains (n = 5) and the single young zircon (n = 1) that is outside statistical uncertainty of the $^{40}Ar/^{39}Ar$ eruption age were excluded from calculations. The $^{206}Pb^*/^{238}U$ dates produce a bimodal distribution (Fig. 4), with mixture model deconvolution peaks at 26.41 ± 0.06 Ma (29%) and 33.96 ± 0.05 Ma (54%) (Sambridge 1994; Ludwig, 2012). Zircon from the Mount Dutton Formation produced $^{206}Pb^*/^{238}U$ dates ranging from 25.13 ± 0.50 Ma to 1823 ± 15 Ma (n = 156). Grains older than 50 Ma were excluded

https://doi.org/10.5194/egusphere-2024-2899
Preprint. Discussion started: 25 September 2024

from calculations (n = 17). The $^{206}Pb^*/^{238}U$ dates of the Mount Dutton Formation produce a fairly unimodal distribution, with a tail to slightly older (>30 Ma) dates. Mixture modeling deconvolution suggests the dominant population is 26.56 ± 0.04 Ma (78%). However, this value is skewed slightly older than the age of the peak (Fig. 4).

The maximum depositional age (MDA) was estimated using maximum likelihood age algorithms (MLA; Galbraith and Laslett, 1993; Vermeesch, 2021). The MLA age for the Kingston Canyon Tuff of 26.13 ± 0.20 Ma (Fig. 5) is in agreement with the $^{40}Ar/^{39}Ar$ eruption age, but is significantly younger than the mixture modeling deconvolution age discussed above. The MLA for the alluvium of the Mount Dutton Formation is 25.24 ± 0.17 Ma (Fig. 5), again significantly younger than the deconvolution age.

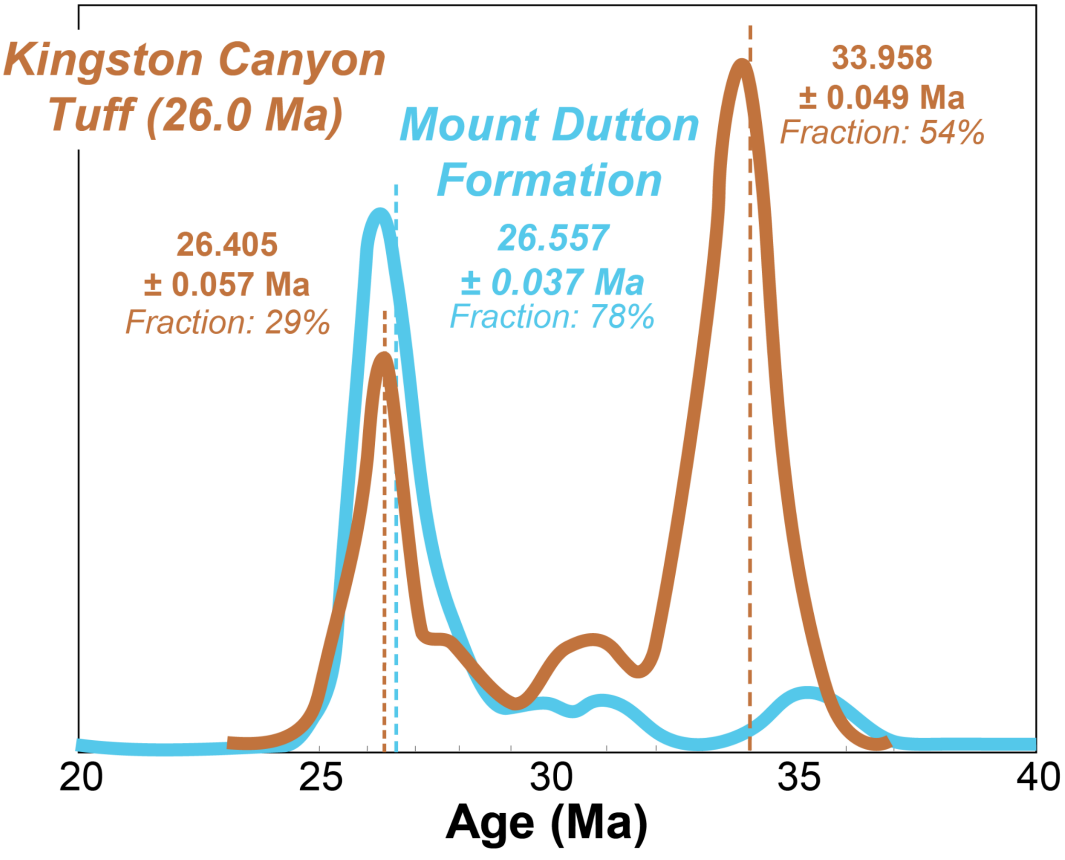

Figure 4: Probability distribution functions for U/Pb zircon dates from the Kingston Canyon Tuff (sample KCT) and overlying alluvium of the Mount Dutton Formation. Mixture modeling deconvolution ages and fraction of total grains are displayed for each mode. The dashed lines mark those deconvolution ages relative to the probability distribution functions.

https://doi.org/10.5194/egusphere-2024-2899
Preprint. Discussion started: 25 September 2024

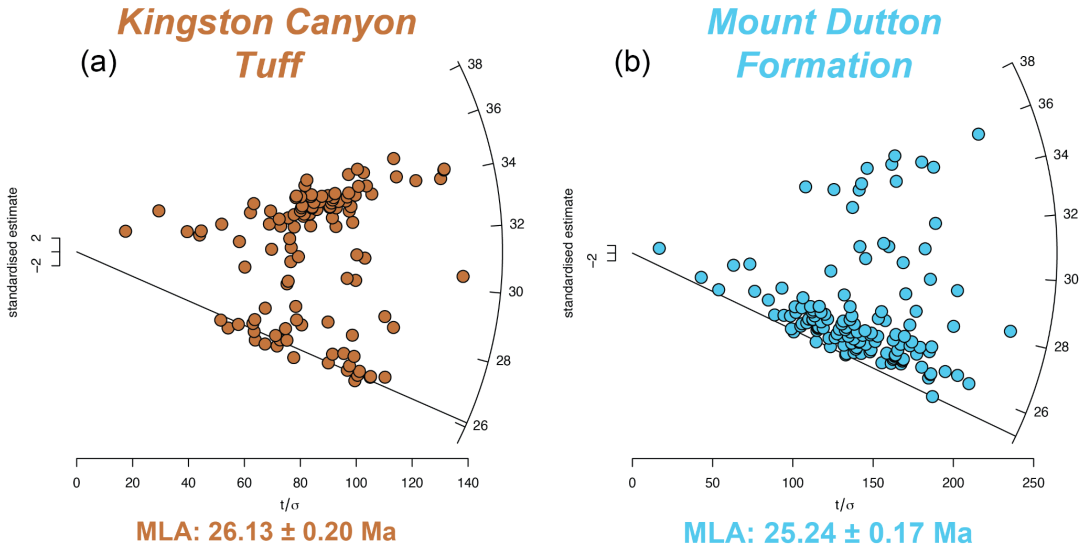

Figure 5: Radial plots of zircon U/Pb data for the (a) Kingston Canyon Tuff and (b) overlying alluvium of the Mount Dutton Formation. MLA: Maximum Likelihood Age. Plots generated using IsoPlotR with the algorithms of Galbraith and Laslett (1993) and Vermeesch (2021) and a logarithmic transformation.

5 Discussion

Emplacement of the SGS was previously constrained to between 23.0 and 25.4 Ma based on a K-Ar age 25.4 ± 0.9 Ma for the tuff of Tibadore, which is the youngest deformed volcanic unit in the SGS, and the 23.0 Ma age of the overlying, undeformed Osiris Tuff (Biek et al., 2019). This age was updated to between 26.2 and 25.1 Ma based on an age of 25.1 Ma for the Antimony Tuff, which post-dates emplacement, and an age of 26.2 Ma for the Buckskin Breccia, the youngest rocks underlying the SGS (Rowley et al., 1994; in press). The breccia itself had not been dated, but included clasts of the Spry and Showalter quartz monzonite intrusions which have similar intrusion dates (Biek et al., 2022). Loffer (2024) estimated an emplacement age of 25.5 Ma based on detrital zircon U/Pb dates from the basal layer of the SGS at two locations. The discovery of pseudotachylyte within the SGS offered an additional opportunity to refine the emplacement age; this work presents an $^{40}Ar/^{39}Ar$ age of 25.25 ± 0.05 Ma for SGS emplacement, consistent with previous estimates but with higher precision. The significant improvement in the plateau age uncertainty for the SGS experiment relative to the pseudotachylyte analysis of Holliday et al. (2022) is because the analyses were performed using the NGX-600 mass spectrometer, which has stable ATONA®-backed Faraday collectors (Mixon et al. 2022) and an incredibly low noise floor (Cox et al., 2020). As such a Bayesian statistical optimization age is not needed. Emplacement occurred approximately 170 kyr after the eruption of the tuff of Tibadore and immediately preceding the eruption of the Antimony Tuff. The slide may have occurred up to 130

https://doi.org/10.5194/egusphere-2024-2899
Preprint. Discussion started: 25 September 2024

kyr prior to the eruption of the Antimony Tuff, or may have occurred near simultaneously, given that the ages and uncertainties for the pseudotachylyte and Antimony Tuff are statistically indistinguishable. Importantly, because the pseudotachylyte had been found within the upper plate associated with subsidiary faults, it has been impossible, until now, to conclusively demonstrate it was formed during slide emplacement. The pseudotachylyte age reported here thus provides tight constraints on the timing of SGS emplacement, and confirms the catastrophic nature of emplacement, consistent with prior interpretations (e.g., Biek et al., 2019; Braunagel et al., 2023).

The bimodal zircon U/Pb distribution of the Kingston Canyon Tuff suggests a significant zircon contribution from a previously crystallized subsurface magma. Xenocrystic inheritance is not observed in the $^{40}Ar/^{39}Ar$ data, possibly due to the small number of grains analyzed. Interestingly, the U/Pb zircon record of the alluvium atop the Kingston Canyon Tuff does not contain a strong 34 Ma signal. This, along with the overall younger MLA of the Mount Dutton alluvium, suggests that the dominant sediment input was derived from a different source. The MLA of the alluvium at the basal layer of the slide is also identical to that of the pseudotachylyte, suggesting that the former land surface was 25.25 Ma when the pseudotachylyte formed.

The Eocene Heart Mountain gravity slide in Wyoming is a comparable feature that is associated with igneous activity of the Absaroka volcanic field. Initiation of the gravity slide has been debated, ranging from incremental movement spanning millions of years (Malone et al. 2014), or catastrophic emplacement spanning several minutes to hours (Craddock et al. 2009). Recently, a lamprophyre suite (breccia, dike, diatreme) was identified at the base of allochthonous rocks. High-precision zircon U/Pb dating of the lamprophyre yielded dates that were identical to those obtained from other basalt cataclasites, leading to the interpretation that the eruption of the diatreme triggered the gravity slide (Malone et al., 2017).

In both the MGSC and Heart Mountain, trigger mechanisms for gravity slides have been poorly understood; however, timing of igneous events relative to the sliding are essential for unraveling the relationship between the two types of events. In the Eocene Heart Mountain gravity slide, igneous activity apparently led to sliding, whereas in the Oligocene SGS, decompression associated with the gravity slide may have initiated the eruption of the Antimony Tuff. However, the timing of the intrusion of the magma body which became the Antimony Tuff is still unknown. Additional insights into the processes associated with Antimony Tuff's pre-eruption magma injection into the upper crust could be unraveled using detailed mineral analyses.

6 Conclusion

New high-precision $^{40}Ar/^{39}Ar$ dating of key units involved in the SGS suggest an emplacement age of 25.25 Ma ± 0.05 Ma. This is approximately two million years prior to the Markagunt gravity slide (Holliday et al., 2022). The emplacement model proposed here is that the slide was initiated from injection of magma, which led to slope failure. This prompted decompression and ultimately the eruption of the 25.19 ± 0.02 Ma Antimony Tuff. The association of magmatic intrusions and gravity slides was also proposed at Heart Mountain, Wyoming, suggesting that large-volume volcanic plateaus may generate these types of catastrophic events more frequently than previously

https://doi.org/10.5194/egusphere-2024-2899
Preprint. Discussion started: 25 September 2024

identified. Further, we begin to resolve the questions about causes for gravity slides (Hacker., 2014) and assess the relationship between igneous activity and mass movements.

Data availability. All data used in this work are provided in the supplementary materials.

Supplementary materials. The supplement is available online.

Author contributions. TR and MH designed the study and performed field collection with BJ, DHM, MJB, RFB, and WAG. BJ and BHM performed $^{40}Ar/^{39}Ar$ and U/Pb data collection, respectively. TR, MH, and VABF performed data analysis. TR prepared the figures and the manuscript, and all authors contributed to the interpretation of results and improvement of the manuscript.

Competing interests. The authors declare no competing interests.

Acknowledgements. We thank the Arizona LaserChron Lab for assistance in analyzing samples for U/Pb data. Samples for this work were obtained from the homelands of the Ute, Southern Paiute and Goshute people.

Financial Support. Funding for this research was provided by the National Science Foundation (EAR-2412838; EAR-2113158, EAR-2113157, EAR-2113155, EAR-2050246).

References

Anderson, J.J., 1993. The Markagunt megabreccia : large Miocene gravity slides mantling the northern Markagunt Plateau, southwestern Utah. Utah Geological Survey, Miscellaneous Publication 93-2. https://doi.org/10.34191/mp-93-2

Biek, R.F, Hacker, D.B., Rowley, P.D., 2014. New constraints on the extent, age, and emplacement history of the early Miocene Markagunt Megabreccia, southwest Utah—the deposit of one of the world's largest subaerial gravity slides, Geology of Utah's far south 43, 565–598.

Biek, R.F., Hacker, D.B., Rowley, P.D., 2017. Catastrophic mega-scale landslide failure of large volcanic fields. Thompson Field Forum. https://doi.org/10.1130/abs/2018rm-314106

Biek, R.F., Rowley, P.D., Anderson, J.J., Maldonado, F., Moore, D.W., Hacker, D.B., Eaton, J.G., Hereford, R., Sable, E.G., Filkorn, H.F., Matyjasik, B., 2015. Geologic map of the Panguitch 30' x 60' quadrangle, Garfield, Iron, and Kane counties, Utah.

https://doi.org/10.5194/egusphere-2024-2899
Preprint. Discussion started: 25 September 2024

306 Biek, R.F., Rowley, P.D., Hacker, D.B., 2022. Utah's ancient mega-landslides—geology, discovery, and guide to
307 Earth's largest terrestrial landslides. Utah Geological Survey Circular 132. https://doi.org/10.34191/c-132
308
309 Biek, R.F., Rowley, P.D., Hacker, D.B., 2019. The Gigantic Markagunt and Sevier Gravity Slides Resulting from
310 Mid-Cenozoic Catastrophic Mega-Scale Failure of the Marysvale Volcanic Field, Utah, USA. Thompson Field
311 Forums.
312
313 Braunagel, M.J., Griffith, W.A., Biek, R.F., Hacker, D.B., Rowley, P.D., Malone, D.H., Mayback, D., Rivera, T.A.,
314 Loffer, Z., Smith, Z.D., 2023. Structural Relationships Across the Sevier Gravity Slide of Southwest Utah and
315 Implications for Catastrophic Translation and Emplacement Processes of Long Runout Landslides. Geochemistry
316 Geophysics Geosystems 24. https://doi.org/10.1029/2022gc010783
317
318 Braunagel, M., Malone, D., Hacker, D., Biek, R., Rivera, T., Loffer, Z., Holliday, M., and Griffith, W. A. (in
319 review) Zircon geochronology records frictional wear during emplacement of the Sevier gravity slide, southwest
320 Utah (USA), submitted to Geology.
321
322 Cox, S.E., Hemming, S.R., Tootell, D., 2020. The Isotopx NGX and ATONA Faraday amplifiers: Geochronology 2,
323 231–243, https://doi .org /10 .5194 /gchron-2-231-2020.
324
325 Craddock, J.P., Malone, D.H., Magloughlin, J., Cook, A.L., Rieser, M.E. Doyle, J.R., 2009. Dynamics of the
326 emplacement of the Heart Mountain allochthon at White Mountain: Constraints from calcite twinning strains,
327 anisotropy of magnetic susceptibility, and thermodynamic calculations. Geological Society of America Bulletin 121,
328 919-938.
329
330 Cunningham, C.G., Steven, T.A., 1979. Mount Belknap and Red Hills calderas and associated rocks, Marysvale
331 volcanic field, west-central Utah, USGS Numbered Series 1468.
332
333 Gehrels, G.E., Pecha, M., 2014. Detrital zircon U-Pb geochronology and Hf isotope geochemistry of Paleozoic and
334 Triassic passive margin strata of western North America. Geosphere 10, 49–65, DOI:10.1130/geos.s.12187251.v1.
335
336 Gehrels, G.E., Valencia, V., Pullen, A., 2006. Detrital zircon geochronology by laser-ablation multicollector ICPMS
337 at the Arizona LaserChron Center. The Paleontological Society Papers 12, 67–76,
338 DOI:10.1017/s1089332600001352.
339
340 Gehrels, G.E., Valencia, V., Ruiz, J., 2008. Enhanced precision, accuracy, efficiency, and spatial resolution of U-Pb
341 ages by laser ablation-multicollector-inductively coupled plasma-mass spectrometry. Geochemistry Geophysics
342 Geosystems 9, DOI:10.1029/2007gc001805.

https://doi.org/10.5194/egusphere-2024-2899
Preprint. Discussion started: 25 September 2024

Granger, H.C., Bauer, H.L., 1950. Preliminary examination of uranium deposits near Marysvale, Piute County, Utah (No. 33). US Geological Survey.

Hacker, D., Biek, R.F., Rowley, P., Griffith, W.A., Malone, D., Rivera, T., 2023. Catastrophic gravity sliding of the Marysvale volcanic field during rapid growth of laccolithic batholiths: insights from the Cenozoic Marysvale gravity slide complex, southwest Utah. https://doi.org/10.1130/abs/2023am-394566

Hacker, D.B., Biek, R.F., Rowley, P.D., 2014. Catastrophic emplacement of the gigantic Markagunt gravity slide, southwest Utah (USA): Implications for hazards associated with sector collapse of volcanic fields. Geology 42, 943–946. https://doi.org/10.1130/g35896.1

Hacker, D.B., Rowley, P.D., Biek, R.F., 2018. Catastrophic collapse features in volcanic terrains: styles and links to subvolcanic magma systems. In: Advances in Volcanology. Springer. https://doi.org/10.1007/11157_2017_1001

Holliday, M.E., Rivera, T., Jicha, B., Trayler, R.B., Biek, R.F., Braunagel, M.J., Griffith, W.A., Hacker, D.B., Malone, D.H., Mayback, D.F., 2022. Emplacement age of the Markagunt gravity slide in southwestern Utah, USA. Terra Nova. https://doi.org/10.1111/ter.12630

Jicha, B.R., Singer, B.S., Sobol, P., 2016. Re-evaluation of the ages of 40Ar/39Ar sanidine standards and supereruptions in the western U.S. using a Noblesse multi-collector mass spectrometer. Chemical Geology 431, 54–66. https://doi.org/10.1016/j.chemgeo.2016.03.024

Kerr, P.F., Brophy, G.P., Dahl, H.M., Green, J., Woolard, L.E., 1957. Marysvale, Utah, Uranium Area: Geology, Volcanic Relations, and Hydrothermal Alteration, Marysvale, Utah, Uranium Area: Geology, Volcanic Relations, and Hydrothermal Alteration (Paul F. Kerr, Gerald P. Brophy, Harry M. Dahl, Jack Green, and Louis E. Woolard, eds.), Geological Society of America 64.

Kuiper, K.F., Deino, A., Hilgen, F.J., Krijgsman, W., Renne, P.R., Wijbrans, J.R., 2008. Synchronizing Rock Clocks of Earth History. Science 320, 500–504. https://doi.org/10.1126/science.1154339

Lee, J.-Y., Marti, K., Severinghaus, J.P., Kawamura, K., Yoo, H.-S., Lee, J.B., Kim, J.S., 2006. A redetermination of the isotopic abundances of atmospheric Ar. Geochimica et Cosmochimica Acta 70, 4507–4512. https://doi.org/10.1016/j.gca.2006.06.1563

https://doi.org/10.5194/egusphere-2024-2899
Preprint. Discussion started: 25 September 2024

Loffer, Z.J., Hacker, D.B., Malone, D.H., Biek, R.F., d Rowley, P. D., 2020, Zircon geochronology of the basal layer of the Sevier gravity slide, Marysvale volcanic field, Utah, USA. Geological Society of America Abstracts with Programs 52, doi: 10.1130/abs/2020RM-346702.

Ludwig, K. R., 2012. User's manual for Isoplot version 3.75–4.15: a geochronological toolkit for Microsoft Excel. Berkeley Geochronological Center Special Publication 5.

Malone, D.H., 1995. Very large debris-avalanche deposit within the Eocene volcanic succession of the northeastern Absaroka Range, Wyoming. Geology 23, 661–664. https://doi.org/10.1130/0091-7613(1995)023<0661:vldadw>2.3.co;2

Malone, D.H., Craddock, J.P., Anders, M.H., Wulff, A.P., 2014. Constraints on the emplacement age of the massive Heart Mountain Slide, Northwestern Wyoming. Journal of Geology 122, 671-685. DOI:10.1086/678279

Malone, D.H., Craddock, J.P., Schmitz, M.D., Kenderes, S., Kraushaar, B., Murphey, C.J., Nielsen, S., Mitchell, T.M., 2017. Volcanic Initiation of the Eocene Heart Mountain Slide, Wyoming, USA. Journal of Geology 125, 439–457. https://doi.org/10.1086/692328

Marchetti, D.W., Stork, A.L., Solomon, D.K., Cerling, T.E., Mace, W., 2020. Cosmogenic 3He exposure ages of basaltic flows from Miller Knoll, Panguitch Lake, Utah: Using the alternative isochron approach to overcome low-gas crushes. Quaternary Geochronology 55, 101035. https://doi.org/10.1016/j.quageo.2019.101035

Mixon, E. E., Jicha, B. R., Tootell, D., Singer, B.S., 2022. Optimizing $^{40}Ar/^{39}Ar$ analyses using an Isotopx NGX-600 mass spectrometer. Chemical Geology 593, 120753. https://doi.org/10.1016/j.chemgeo.2022.120753

Palmer, B.A., Walton, A.W., 1990. Accumulation of volcaniclastic aprons in the Mount Dutton Formation (Oligocene-Miocene), Marysvale volcanic field, Utah, Geological Society of America Bulletin 102, 6, 734–748.

Pullen, A., Ibanez-Mejia, M., Gehrels, G., Giesler, D., Pecha, M., 2018. Optimization of a laser ablation-single collector-inductively coupled plasma-mass spectrometer (Thermo Element 2) for accurate, precise, and efficient zircon U-Th-Pb geochronology. Geochemistry, Geophysics, Geosystems 19, 3689-3705. DOI:10.1029/2018GC007889.

Rowley, P.D., Anderson, J.J., WIlliams, P., 1975. A Summary of Tertiary Volcanic Stratigraphy of the Southwestern High Plateaus and Adjacent Great Basin, Utah.

Rowley, P.D., Biek, R.F., Hacker, D.B., Vice, G.S., McDonald, R.E., Maxwell, D.J., Fasselin, R., Dustin, J., Cunningham, C.G., Steven, T.A., Anderson, J.J., Ekren, B.E., Machete, M.N., Wardlaw, B.R., Smith, Z.D., Kirby,

https://doi.org/10.5194/egusphere-2024-2899
Preprint. Discussion started: 25 September 2024

S.M., Knudsen, T.R., Kleber, E.J., Hiscock, A.I., Malone, D.H., Rivera, T.A., Jicha, B.R., *Interim geologic map of the Beaver 30' x 60' quadrangle, Beaver, Piute, Iron, and Garfield Counties, Utah*, (in press.).

Rowley, P.D., Cunningham, C.G., Steven, T.A., Mehnert, H.H., Naeser, C.W., 1997. Cenozoic Igneous and Tectonic Setting of the Marysvale Volcanic Field and Its Relation to Other Igneous Centers in Utah and Nevada, in: Friedman, J.D., Huffman, C. (Eds.), Laccolith Complexes of Southeastern Utah: Time of Emplacement and Tectonic Setting-Workshop Proceedings, Laccolith Complexes of Southeastern Utah. U.S. Geological Survey Bulletin 2158, pp. 167–201.

Rowley, P.D., Cunningham, C.G., Steven, T.A., Workman, J.B., Anderson, J.J., Theissen, K.M., 2002. Geologic Map of the Central Marysvale Volcanic Field, Southwestern Utah. Geological Investigations Series I-2645-A.

Rowley, P.D., Mehnert, H.H., Naeser, C.W., Snee, L.W., Cunningham, C.G., Steven, T.A., Anderson, J.J., Sable, E.G., Anderson, R.E., 1994. Isotopic ages and stratigraphy of Cenozoic rocks of the Marysvale Volcanic Field and adjacent areas, west-central Utah. U.S. Geological Survey Bulletin 2071.

Sable, E.G., Maldonado, F., 1997. Breccias and megabreccias, Markagunt Plateau, southwestern Utah: Origin, age, and transport directions, United States Geological Survey Bulletin 2153, 151–176.

Sambridge, M.S., Compston, W., 1994. Mixture modeling of multi-component data sets with application to ion-probe zircon ages. Earth and Planetary Science Letters 128, 373–390, doi:10.1016/0012-821x(94)90157-0.

Steven, T.A., Cunningham, C.G., Naeser, C.W., Mehner, H., 1977. Revised stratigraphy and radiometric ages of volcanic rocks and mineral deposits in the Marysvale area, west-central Utah, USGS Open File Report 77-569.

Steven, T.A., Rowley, P.D., Cunningham, C.G., 1984. Calderas of the Marysvale Volcanic Field, west central Utah, Journal of Geophysical Research 89, no. B10, 8751.

Sundell, K.E., Gehrels, G.E., Pecha, M.E., 2021. Rapid U-Pb geochronology by laser ablation multi-collector. Geostandards and Geoanalytical Research 45, 37-57. DOI:10.1111/ggr.12355.

Taylor, A.O., Anderson, T.P, O'Toole, W.L., Waddell, G.G., Gray, A.W., Douglas, H., Cherry, C.L., Caywood, R.M., 1951. Geology and Uranium Deposits of Marysvale, Utah, Interim Report on the Producing Area 896, Technical Information Service.

https://doi.org/10.5194/egusphere-2024-2899
Preprint. Discussion started: 25 September 2024

449 Wender, L.E., Nash, W.P., 1979. Petrology of Oligocene and early Miocene calc-alkalic volcanism in the Marysvale
450 area, Utah: Summary. Geological Society of America Bulletin 90, 2–3. https://doi.org/10.1130/0016-
451 7606(1979)90<2:pooaem>2.0.co;2
452
453 Zamanialavijeh, N., Hosseinzadehsabeti, E., Ferré, E.C., Hacker, D.B., Biedermann, A.R., Biek, R.F., 2021.
454 Kinematics of frictional melts at the base of the world's largest terrestrial landslide: Markagunt gravity slide,
455 southwest Utah, United States. Journal of Structural Geology 153, 104448.
456 https://doi.org/10.1016/j.jsg.2021.104448
457